Brittle Versus Ductile Failure of a Lead-Free Single Solder Joint Specimen Under Intermediate Strain Rate

Jianping Jing, Feng Gao, Janine Johnson, Frank Z. Liang, Richard L. Williams, and Jianmin Qu

Abstract—The failure mode of Sn-4.0Ag–0.5Cu solder joints under the intermediate strain rates is explored. Tensile and shear tests were performed on miniature solder joints at two different displacement rates, i.e., 5 and 50 mm/s. For the uniaxial tensile test, brittle failure occurred at the intermetallic compound (IMC)/Cu pad interface on the board side under both loading rates. However, for shear loading at 5 mm/s, ductile failure along the solder matrix was detected. With the increase of the shear loading rate up to 50 mm/s, the failure mode is converted into the (ductile + brittle) mixed mode. Numerical simulation results based on the extracted elastic–plastic solder properties indicate that the maximum stress concentration is located at the interfaces of the board side, which indicates the weak position of the crack initiation. The plastic deformation of the solder alloy is significantly suppressed at 50 mm/s loading rate. The amplitude of the solder plastic deformation under shear loading is much greater than that for the tensile test. Furthermore, most plastic deformation under shear loading is in the solder alloy adjacent to solder/IMC interface of the board side and no visible plastic deformation is detected in the middle of solder ball, which results in cohesive failure at the rate of 5 mm/s and the (ductile + brittle) mixed failure mode at the rate of 50 mm/s.

Index Terms—Failure mode, plastic deformation, single solder joint, Sn–4.0Ag–0.5Cu solder.

I. INTRODUCTION

NOWADAYS, Sn–Ag–Cu lead-free solders have been considered as the leading candidates to replace the conventional Sn–Pb solders owing to their good manufacturability, creep resistance, and thermomechanical fatigue resistance

J. Jing is with the State Key Laboratory of Mechanical Systems and Vibration, Shanghai JiaoTong University, Shanghai 200000, China (e-mail: jianpj@gmail.com).

F. Gao and J. Qu are with the George W. Woodruff School of Mechanical Engineering, Georgia Institute of Technology, Atlanta, GA 30332 USA. They are also with McCormick School of Engineering and Applied Science, Northwestern University, Evanston, IL 60208 USA (e-mail: feng-gao@northwestern.edu; j-qu@northwestern.edu).

J. Johnson was with the George W. Woodruff School of Mechanical Engineering, Georgia Institute of Technology, Atlanta, GA. She is now with the Lincoln Laboratory, Massachusetts Institute of Technology, Lexington, MA 02421-6426 USA (e-mail: janine.johnson@gatech.edu).

F. Z. Liang and R. L. Williams are with Intel Corporation, Hillsboro, OR 97124 USA (e-mail: frank.z.liang@intel.com; richard.l.williams@intel.com).

Color versions of one or more of the figures in this paper are available online at http://ieeexplore.ieee.org.

[1], [2]. However, a crucial reliability issue of the lead-free solder joints has emerged. That is, compared to Sn–Pb solder joints, the lead-free solder joint exhibits deterioration in performance under shock/impact loading. In the meantime, the proliferation of portable electronic devices, such as cellular phones and laptop computers, makes the drop in performance of the solder joint very important.

The local strain rate within a solder joint at the drop condition may differ from 1 s^{-1}–1000 s^{-1}, depending on the drop height, orientation, surface rigidity, etc. [3]. For board-level drop test or single ball impact test, a number of studies have been reported [4]–[6]. In particular, the Hopkinson bar has been utilized to explore the mechanical behavior under high strain rates (500–3000 s^{-1}) [7], [8]. Recently, it has been found that the solder properties strongly depend on the solder joint height [9].

This paper is devoted to the study of the properties of a miniature solder ball, which are extracted directly from the force–displacement measurement data. The solder joint failure mode under different loading conditions is then discussed on the basis of numerical simulation results.

II. SINGLE SOLDER JOINT (SSJ) SAMPLE PREPARATION

The package and printed circuit board (PCB) were soldered using the commercial Sn–4.0Ag–0.5Cu (SAC405) lead-free solder alloy. The SSJ was then made through the singulation process from an assembled PCB, so that the SSJ specimen matched with the targeted ball grid array solder joint. The dimensions of the SSJ are shown in Table I. Fig. 1 illustrates a typical SSJ that is assembled for the tensile loading test.

Intermetallic compounds (IMCs) are formed at the interfaces of both the package and board sides, as illustrated in Fig. 2(a). Several kinds of IMCs, such as block-like Cu_6Sn_5 and needle-like Ag_3Sn, are detected in the solder matrix. The formation of large-sized Ag_3Sn plates is due to the relatively high initial Ag content. The (β-Sn + Ag_3Sn) and (β-Sn + Ag_3Sn + Cu_6Sn_5) eutectic phases are networked with dendrite-shaped β-Sn structures. The cross-polarized image in Fig. 2(b) reveals that the solder ball consists of a limited number of grains with different orientations, although the polarized image cannot detail the grain orientation as in orientation imaging microscopy. Accordingly, the solder alloy is a nonhomogeneous microstructure and possesses several grains with different orientations. The properties of the SAC405
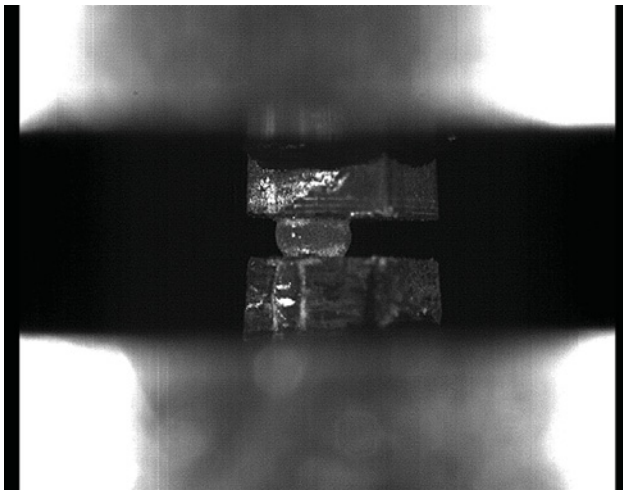
Fig. 1.   Typical SSJ assembled for testing.

TABLE I
DIMENSIONS OF SINGLE SOLDER JOINT SPECIMEN

PCB Cu pad interface diameter (μm)	450
Substrate pad interface diameter (μm)	500
Solder ball diameter (μm)	550
Solder joint height (μm)	355
Substrate/PCB (width $\times$ depth) (μm)	1160 $\times$ 1300

alloy in our study were carefully estimated. The following section describes the methodology to extract the elastic–plastic properties of solder alloy.

A. Experimental Test Procedure

High-speed testing was carried out on a home-developed test frame, with grips developed specifically for the SSJ test. Before testing, platens were made for easy removal and installation of the solder joints into the grips. Each platen consists of bottom and top with a planar surface for sample attachment. As illustrated in Fig. 1, the internal angles θ of these planes were 0° and 90°, where 0° corresponded to a uniaxial tensile test and 90° corresponded to a shear test.

After removing the debris from the solder joint, the sample was presoaked in distilled water and then was glued onto a platen with the substrate side down and allowed to cure for 15 min. This platen was placed in the grips on the actuator side. Then the circuit board was affixed to the opposite platen by raising the frame until the circuit board and the top platen were connected by a thin film of glue. A second cure time of 15 min was applied. After the actuator was started at the desired speed, load was not applied to the solder joint until an additional alignment cylinder on the actuator side was fully extended. The load displacement sampling rate was 2×10^{-4} s for 5 mm/s and 4×10^{-5} s for 50 mm/s, which ensured that the continuous force–displacement data were recorded accurately. After the test, the cross-sectional microstructure was observed by optical microscopy.
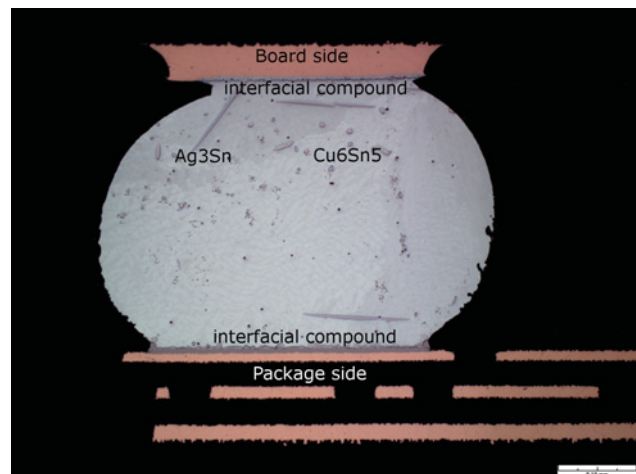
(a)
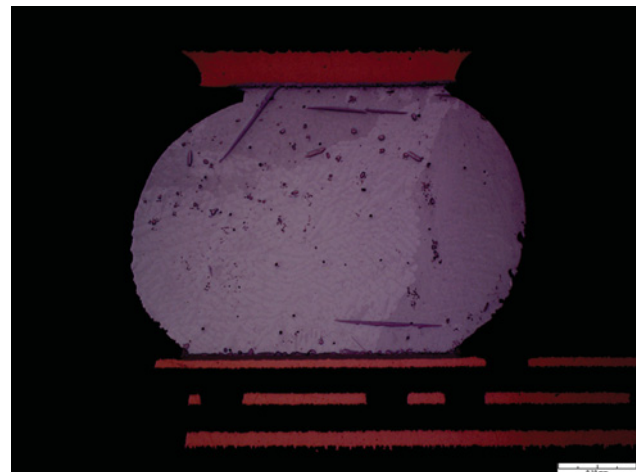
(b)

Fig. 2.   Optical micrographs of a SSJ. (a) SSJ before testing. (b) Corresponding cross-polarized image.

B. Test Results: Force Versus Displacement Curves

The test data at two loading rates (i.e., 5 and 50 mm/s), which are shown in Fig. 3, were employed to assess the mechanical properties of solder by reverse calculations. In the calculation, the measured displacements shown in Fig. 3 were used as prescribed loading conditions on the top surface of the specimen, the reaction force at the bottom of the specimen was then calculated by numerical analysis. When the calculated reaction forces fitted the measured forces, the mechanical properties of solder alloy at different loading rates were then obtained.

Fig. 4 displays the derived properties of SAC405 solder alloy in this paper by the reverse analysis of the recorded force–displacement data. The properties presented here were anticipated to include several aspects, such as microstructure, solder ball size effect, etc. It has been reported that the grain orientation in a small-size solder ball will affect the stress and strain distributions [10]. Due to the diverse solder ball microstructures in an assembled PCB, the grain orientation effect is not specified in this paper. Overall, it can be seen that at the higher displacement rate, namely, 50 mm/s,
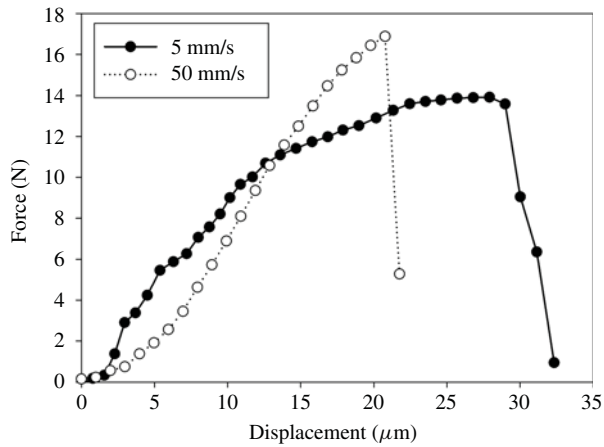
Fig. 3. Relation of the force versus displacement at different loading rates (5 and 50 mm/s).
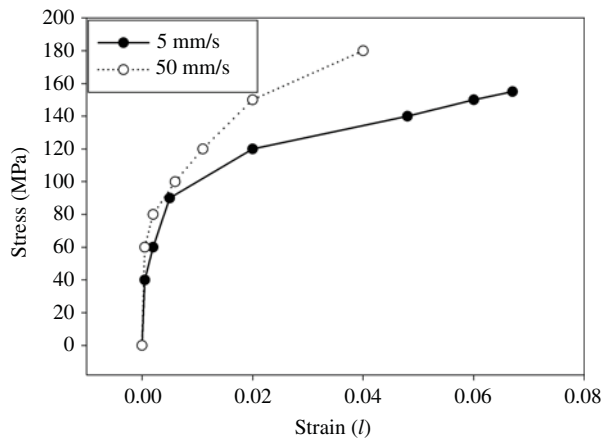

Fig. 4. Derived stress versus strain relation of the solder alloy at different tensile loading rates.

the yield strength of SAC405 solder alloy becomes greater. The Young's modulus at 50 mm/s is also slightly elevated. This in turn affects the plastic deformation behavior of the solder alloy, which will be addressed later. The properties were then adopted as the input parameters for the subsequent numerical simulation, in order to reveal the weak position for the potential crack initiation and propagation qualitatively of an SSJ which was subjected to different loading conditions.

III. RESULTS AND DISCUSSION: BRITTLE VERSUS DUCTILE FAILURE

A. Load Rate 5 mm/s

For uniaxial tensile loading at 5 mm/s, the brittle failure along the IMC/board pad interface is dominant, as shown in Fig. 5(a) and (b). These interfaces were found to be the weak positions for the interconnections under high strain rate loading, which was partially attributed to the brittle characteristics of the IMCs. It is interesting that the edges of the fracture interface show the ductile behavior. Remarkable plastic deformation was likely to occur at these edge zones, which indicated that the crack might initiate from the triple joint of the solder/IMC/Cu interfaces rather than from the
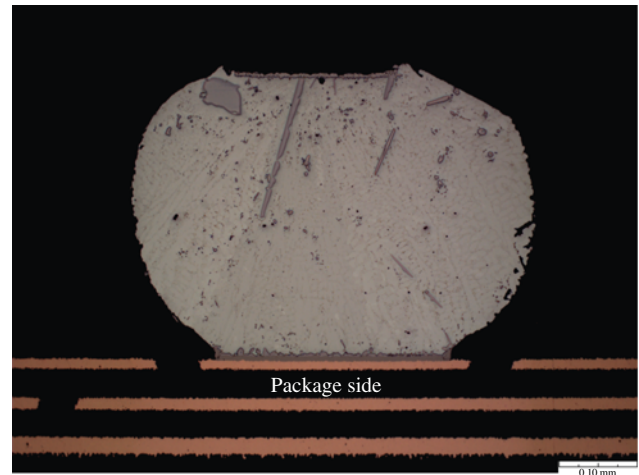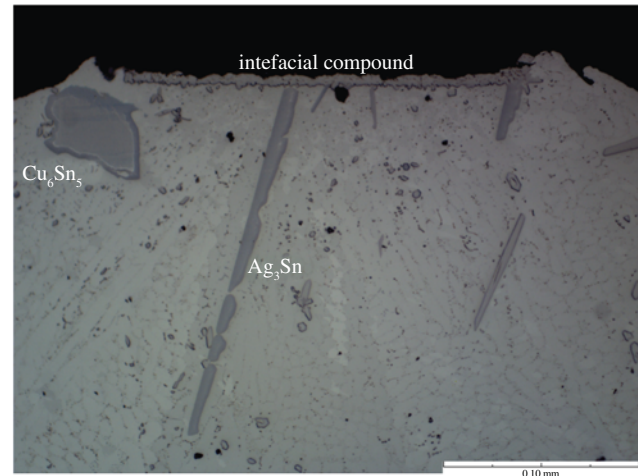
Fig. 5. Microstructure of solder joint at package side after the uniaxial tensile test (5 mm/s). (a) Package side solder joint after testing. (b) Close-up of the fracture surface.

TABLE II
ISOTROPIC MATERIAL PARAMETERS

	Solder	Copper	SM	Ni	Cu_6Sn_5
E (GPa)	53 (50 mm/s) 50 (5 mm/s)	117	24	203	119
v	0.34	0.34	0.4	0.34	0.29

IMC/Cu interface. A different failure mode took place for shear loading at 5 mm/s. Fig. 6(a) and (b) depict the fracture surfaces at the package side and board side, respectively, which exhibit a ductile-controlling failure. Clearly, the failure develops along the solder alloy matrix, and the dramatic deformation of the solder alloy also occurs at the fracture surface.

Based on the failure mode and the microstructure observation, it is inferred that the deformation of the solder alloy near the solder/IMC interface under the shear loading is more severe than that under tensile loading. Moreover, the interface at the board side is more susceptible to the stress concentration and the subsequent crack initiation. A numerical simulation was therefore performed to seek a qualitative explanation.

TABLE III
ANISOTROPIC MATERIAL PARAMETERS

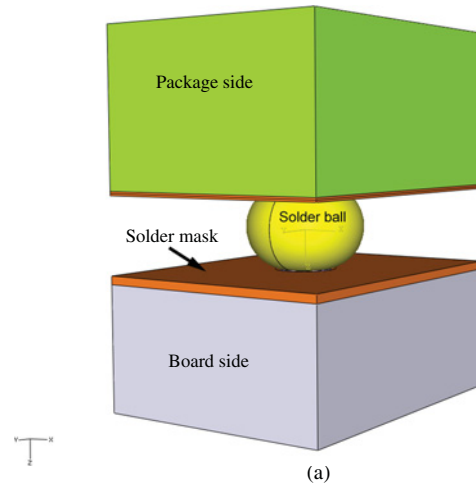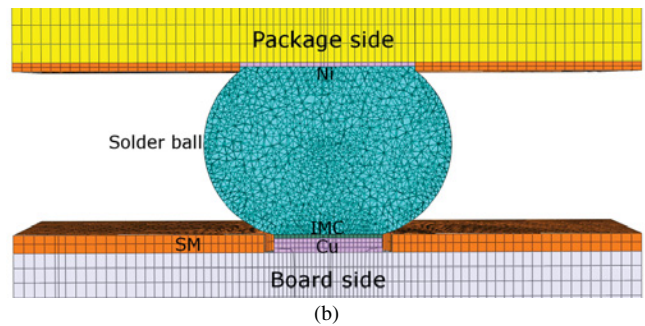|	$E1, v1$ (GPa, /)	$E2, v2$ (GPa, /)	$E3, v3$ (GPa, /)	$G12$ (GPa)	$G13$ (GPa)	$G23$ (GPa)
PCB	22, 0.28	22, 0.28	4.8, 0.18	8.0	4.0	4.0
Substrate	21, 0.3	21, 0.3	6.0, 0.2	8.0	4.0	4.0
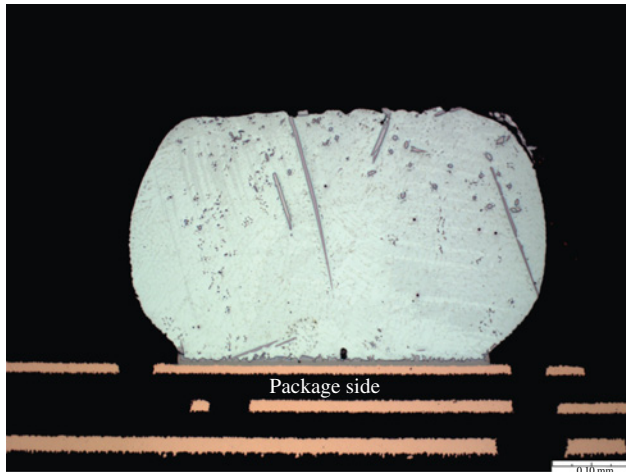
(a)
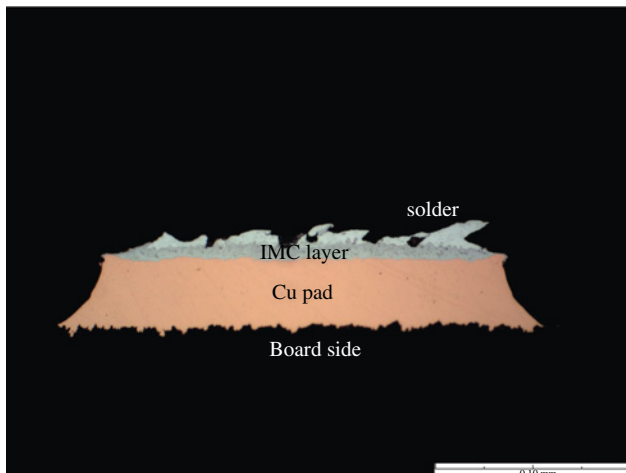
(b)

Fig. 6. Microstructure of solder joint at both sides after the shear test (5 mm/s). (a) Package side solder joint after testing. (b) Fracture surface at the board pad.

(a)

(b)

Fig. 7. (a) 3-D SSJ model for the finite element simulation. (b) Close-up view of the interfaces of a SSJ.

Fig. 7(a) depicts a 3-D SSJ model for the numerical simulation, while Fig. 7(b) shows a close-up view of the interfaces in an SSJ. Tables I–III display the SSJ dimensions and material properties, while the elastic–plastic properties of SAC405 solder joint are governed by the plots in Fig. 4. The numerical calculation was performed using the ABAQUS software. In order to simulate the loading process, the bottom surface of an SSJ model was frozen in the x, y, and z directions, which mimics the situation where the bottom of the specimen is glued to a rigid substrate. The velocities, i.e., 5 and 50 mm/s, are prescribed for all the nodes on the top surface of a finite element system. The velocity normal to the top surface represents a simple tensile loading ($\theta = 0°$), while

the velocity parallel to the top surface denotes a pure shear test ($\theta = 90°$). It should be noted that, for shear loading, the top and bottom surfaces are constrained to be parallel during the entire process to avoid any rotation, which is consistent with the actual shear test loading condition. The IMC with a few micrometers at the board side is included in the model. The IMC is Cu_6Sn_5 at the board side. And the IMC layer is simplified as having a flat morphology in the simulation models.

Figs. 8 and 9 illustrate the stress and equivalent plastic strain fields under the uniaxial tensile and shear loading at the rate of 5 mm/s, respectively. It can be seen that for both tensile and shear loading, the maximum stress concentration is at the edge of solder/IMC/Cu pad interfaces of the board side. Figs. 8(c) and 9(c) show the enlarged stress field at the interface domain of the board side for a clear view. At the package side, the stress concentration amplitude is much lower. This indicates that the solder/IMC/Cu interfaces at the board side are the potential sites for damage initiation, which is consistent with the experimental observation. However, the failure modes for
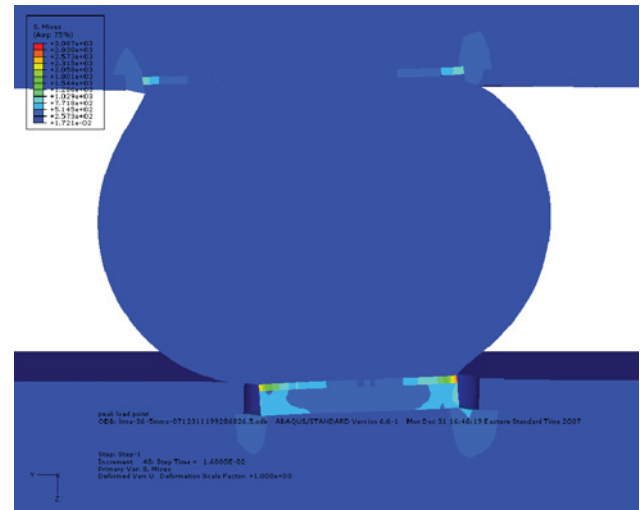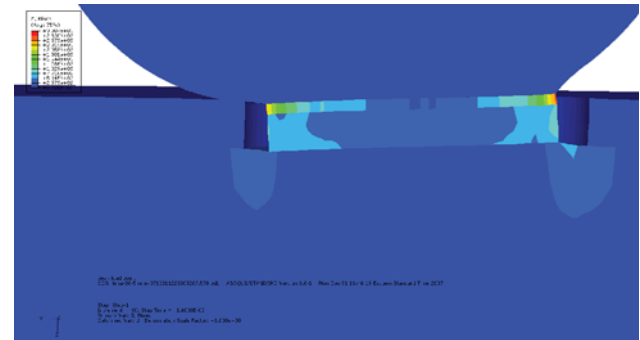
(a)

(b)
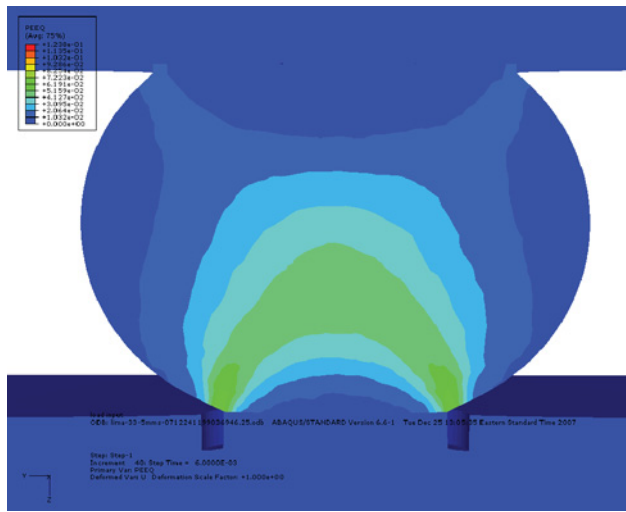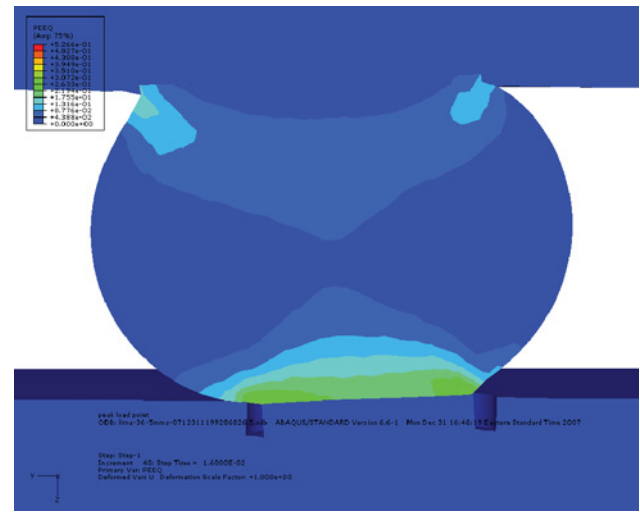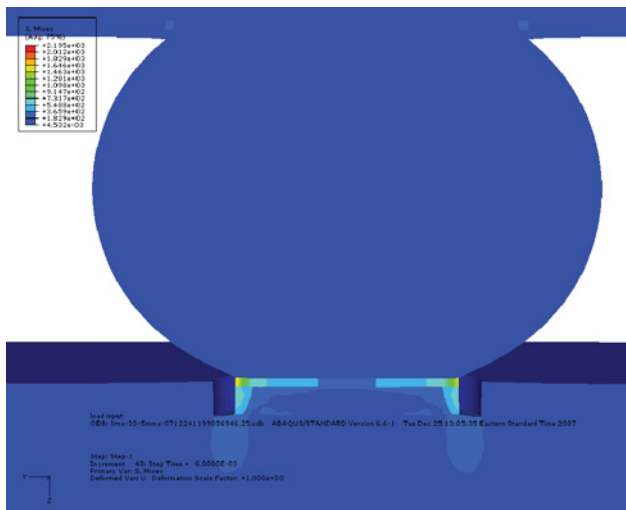
(c)

Fig. 8. Simulated results for the uniaxial tensile loading (5 mm/s). (a) Equivalent plastic strain field. (b) Mises stress field. (c) Enlarged stress field at the interface of the board side.

Fig. 9. Simulated results for the shear loading (5 mm/s). (a) Equivalent plastic strain field. (b) Mises stress field. (c) Enlarged stress field at the interface of the board side.

tensile and shear loading are quite different, which is due to the different distributions of plastic deformation of the solder alloy. Under the tensile loading (rate = 5 mm/s), the maximum plastic deformation is mainly located at the edge of the interface between the solder alloy and the IMC layer, and increases gradually toward the solder alloy. It should be noted

that, at the board side, the solder alloy adjacent to the IMC layer is not subjected to a significant plastic deformation. For the shear test, it is interesting that the plastic deformation of the solder alloy adjacent to the IMC layer is also altered. That is, most of the plastic zone lies on the solder alloy adjacent to the solder/IMC interface and decreases gradually toward the
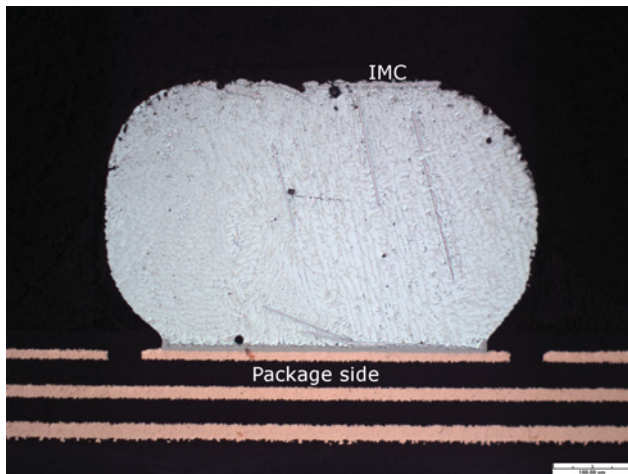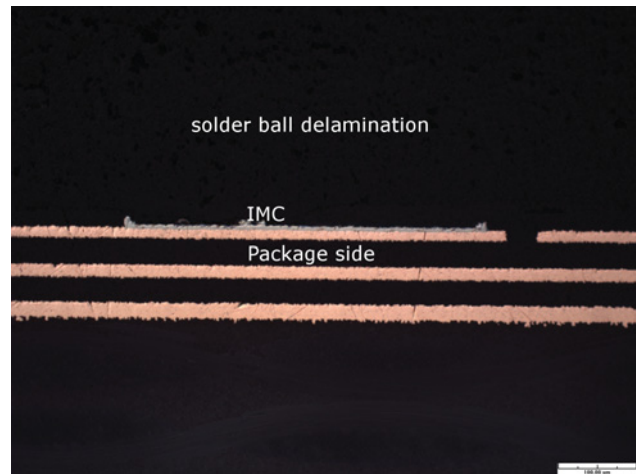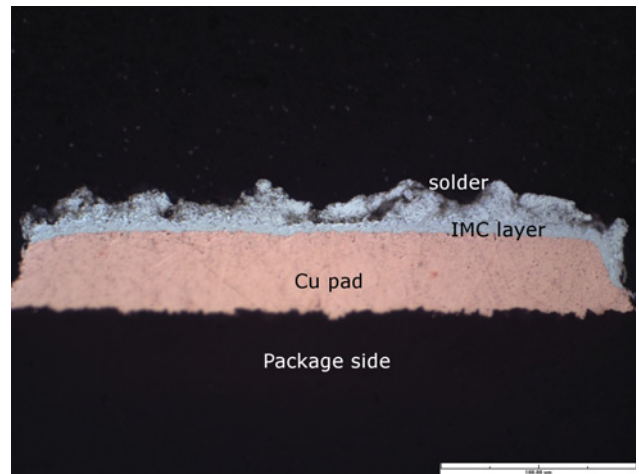
(a)
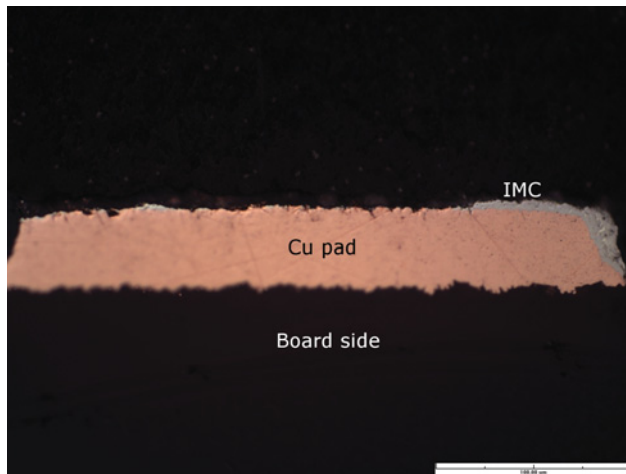
(b)

Fig. 10. Microstructure of solder joint at both sides after the uniaxial tensile loading (50 mm/s). (a) Package side solder joint after testing. (b) Residual pad at the board side.


(a)

(b)

Fig. 11. Microstructure of solder joint at both sides after the shear loading (50 mm/s). (a) Solder ball delamination at the package side. (b) Fracture surface at the board pad.

inner solder matrix. In the middle area of the solder alloy, there is almost no visible plastic deformation, which in turn implies that it will be more effective in releasing the solder/IMC interfacial energy by the solder alloy. In fact, this phenomenon has been studied by the so-called extrinsic toughening, which refers to a toughening mechanism by the reduction of effective or net crack driving force that the crack tip actually experiences through various energy dissipation processes without increasing inherent fracture resistance of material or interface [11], [12]. The extrinsic toughening is concerned with various energy dissipation processes in the zone surrounding the crack to increase the energy consumed per unit extension of crack length. Extrinsic toughening often plays a dominant role in the overall fracture resistance, especially for brittle materials or an interface in which intrinsic toughening is often ineffective.

At a solder joint, the interface fracture resistance is known to be determined by two distinct energy-absorbing processes: the near-crack tip work of fracture (intrinsic fracture resistance) and various energy dissipation processes in a zone surrounding the interfacial crack [11]. The energy dissipation processes

arise from the plasticity of the adjacent ductile layer, which tends to dissipate the applied crack driving force so that the net driving force is reduced. It has been reported that the plastic deformation in the adjacent ductile layer has significant toughening effects on the interface fracture [12]. In the solder joint, this ductile layer is the solder ball, which easily shows plastic deformation under loading while the brittle material is IMC or Cu. If the solder plasticity adjacent to the IMC is enhanced, a higher resistance to interfacial crack propagation under loading will be achieved as more energy is dissipated by the ductile solder. Therefore, under shear loading, it will make the crack propagation shift up to the solder matrix and result in an entire cohesive failure within the solder alloy. This is also consistent with the experimental results shown in Fig. 6(b). In the meantime, it can be concluded that the SSJ is more susceptible to brittle interfacial fracture along the IMC/Cu interface under tensile loading due to the small plastic deformation of solder alloy adjacent to the IMC layer. Although the grain orientations of solder ball may alter the stress and plastic deformation contours, our results can still shed the light to estimate the failure mode qualitatively.
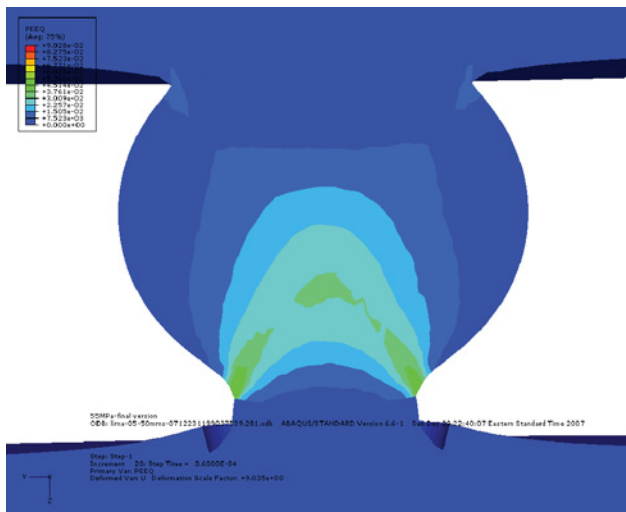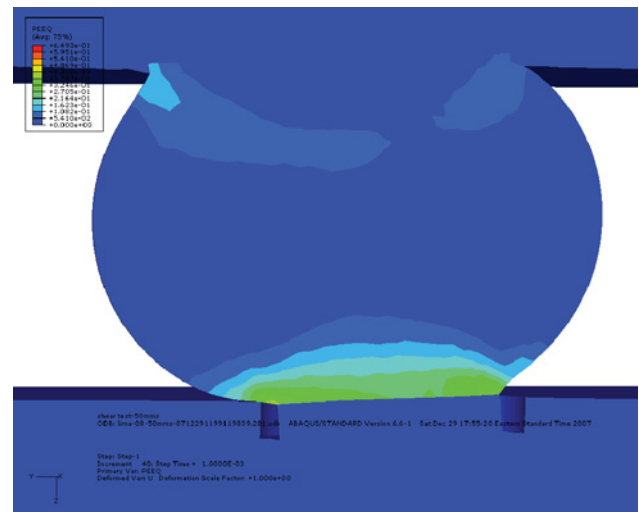
(a)
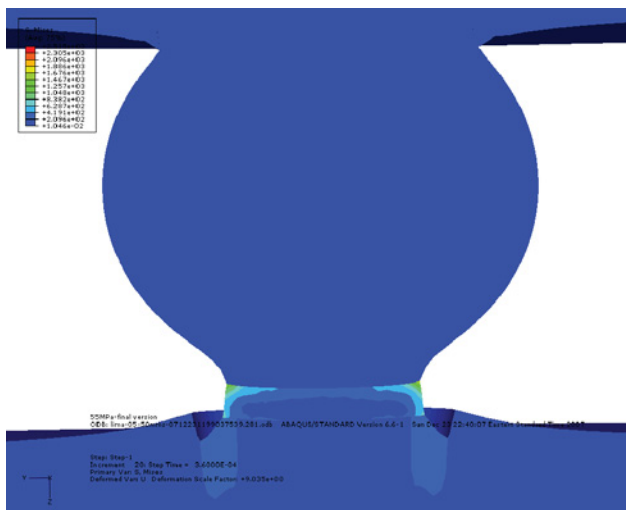
(b)

Fig. 12. Simulated results under the uniaxial tensile loading (50 mm/s). (a) Equivalent plastic strain field. (b) Mises stress field.

(a)

(b)

Fig. 13. Simulated results under the shear loading (50 mm/s). (a) Equivalent plastic strain field. (b) Mises stress field.
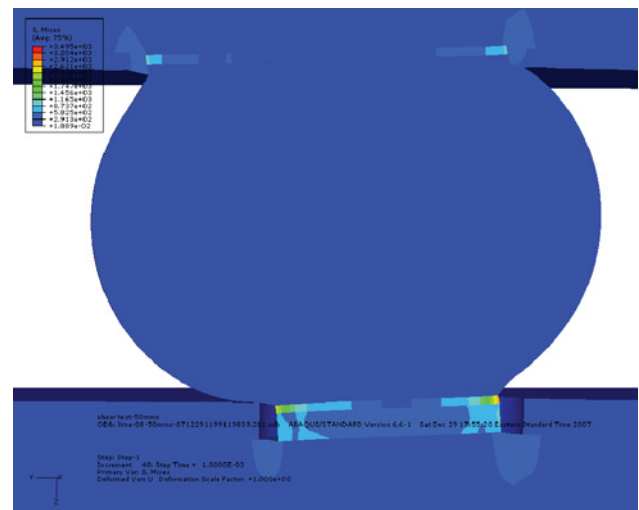
B. Load Rate 50 mm/s

At the rate of 50 mm/s, the brittle failure is still dominant for the tensile loading, as shown in Fig. 10(a) and (b). The failure development mainly occurs along the IMC/Cu pad interface of the board side. For the shear loading at the rate of 50 mm/s, most failure of the SSJ is still at the board side. However, solder ball delamination also takes place at the package side of a few specimens, as illustrated in Fig. 11(a). For the failure at the board side as shown in Fig. 11(b), the failure propagates along the path of the solder matrix + solder/IMC interface. Compared with the tensile case, the cohesive failure tends to contribute to the overall failure process. Therefore, the (ductile + brittle) mixed failure mode is suggested for the shear test at the rate of 50 mm/s.

Figs. 12 and 13 show the stress and equivalent plastic strain fields under the tensile and shear loading at the rate of 50 mm/s. Under shear loading at the rate of 50 mm/s, most of the plastic strain zone still lies on the solder matrix along the solder/IMC, which is still effective in releasing the solder/IMC interface energy. However, compared to the cases at 5 mm/s shown in Fig. 9(a), the amplitude of the plastic deformation is suppressed as a result of the elevated Young's modulus and yield strength of SAC405 lead-free solder alloy, as demonstrated in Fig. 4. Accordingly, the brittle failure will participate in the overall failure mode, as shown in Fig. 11(b). The maximum stress concentration is still probed at the solder/IMC/Cu interfaces of the board side, which indicates that the failure is more susceptible to occur at these interfaces. However, compared to Fig. 12(b), a striking phenomenon is that, under shear loading, remarkable stress concentration takes place at the interface of the package side, as illustrated in Fig. 13(b). This will increase the potential failure at the package side, depending on the toughness of the interface, as shown in Fig. 11(a). Thus, during the shear test, most of the failures occur at the interface of the board side, whereas a higher loading rate (e.g., 50 mm/s) is also capable of triggering a failure at the interface of the package side.

IV. Conclusion

The failure behavior of an SSJ was explored on the basis of microstructural observation and the numerical simulation. The following conclusions could be arrived at:

1) the SAC405 lead-free solder alloy properties exhibit strong dependence on the loading rates. The properties were extracted here on the basis of the *in situ* testing, which included the contributions of both the microstructure and the solder ball size effects. Overall, at higher loading rates (e.g., 50 mm/s), greater Young's modulus and yield strength were achieved;

2) the SSJ subjected to tensile or shear loading shows different failure modes. For uniaxial tensile loading, the brittle failure at the interface of board side is dominant under the rates of 5 and 50 mm/s. However, for the shear testing, it is converted into cohesive failure mode at the rate of 5 mm/s, whereas the failure develops along the path of solder matrix + solder/IMC at the loading rate of 50 mm/s due to the higher Young's modulus and yield strength;

3) for all the cases discussed here, the maximum stress concentration takes place at the interface of the board side, which reveals the weak site of the crack initiation. In particular, compared to tensile loading, a remarkable stress concentration is also generated at the interface of the package side under shear loading, which enhances the failure possibility at the package side to some extent;

4) under uniaxial tensile loading, the maximum plastic deformation is located at the interface edge of the board side and decreases gradually toward the solder matrix, while the solder alloy adjacent to the solder/IMC interface is not subjected to significant plastic deformation. Under the shear loading, the majority of the plastic deformation lies on the solder adjacent to the solder/IMC interface and almost no visible plastic deformation is probed in the middle area of the solder ball. The different distribution and amplitude of the solder alloy plastic deformation are responsible for the different failure modes of an SSJ model under tensile and shear loading.

V. Acknowledgment

References

[1] S. L. Choi, A. W. Gibson, J. L. McDougall, T. R. Bieler, and K. N. Subramanian, *Design Reliability of Solders and Solder Interconnections*, R. K. Mahidhara, D. R. Fear, and K. L. Murty, Eds. Warrendale, PA: TMS, 1977, pp. 241–245.

[2] R. W. Neu, D. T. Scott, and M. W. Woodmansee, "Thermomechanical behavior of 96Sn-4Ag and casting alloy," *Trans. ASME J. Electron. Packag.*, vol. 123, no. 3, pp. 238–246, Sep. 2001.

[3] X. Long, I. Dutta, V. Sarihan, and D. R. Frear, "Deformation behavior of Sn-3.8Ag-0.7Cu solder at intermediate strain rates: Effect of microstructure and test conditions," *J. Electron. Mater.*, vol. 37, no. 2, pp. 189–200, 2008.

[4] J.-W. Kim and S.-B. Jung, "Reexamination of the solder ball shear test for evaluation of the mechanical joint strength," *Int. J. Solids Struct.*, vol. 43, nos. 7–8, pp. 1928–1945, Apr. 2006.

[5] O. van der Sluis, R. B. R. van Silfhout, R. A. B. Engelen, W. D. van Driel, and G. Q. Zhang, "A numerical method for efficient failure modelling of 3-D bond pad structures," in *Proc. Electron. Comp. Technol. Conf.*, Reno, NV, 2007, pp. 235–241.

[6] C.-L. Yeh and Y.-S. Lai, "Effects of solder alloy constitutive relationships on impact force responses of package-level solder joints under ball impact test," *J. Electron. Mater.*, vol. 35, no. 10, pp. 1892–1901, 2006.

[7] C. R. Siviour, D. M. Eilliamson, S. J. P. Palmer, S. M. Walley, W. G. Proud, and J. E. Field, "Dynamic properties of solders and solder joints," *J. Phys., IV*, vol. 110, no. 1, pp. 477–482, Sep. 2003.

[8] K. Kaminishi, T. Sekine, T. Maruichi, and S. Osaki, "Impact tensile characteristics of Sn-3.0Ag-0.5 Cu lead-free solder," *Trans. Jpn. Soc. Mech. Eng.*, vol. 70, no. 690, pp. 266–272, 2004.

[9] P. Zimprich, U. Saeed, A. Betzwar-Kotas, B. Weiss, and H. Ipser, "Mechanical size effects in miniaturized lead-free solder joints," *J. Electron. Mater.*, vol. 37, no. 1, pp. 102–109, 2008.

[10] J. C. Gong, C. Q. Liu, P. P. Conway, and V. V. Silberschmidt, "Micromechanical modelling of SnAgCu solder joint under cyclic loading: Effect of grain orientation," *Comput. Mater. Sci.*, vol. 39, no. 1, pp. 187–197, Mar. 2007.

[11] D. Suh, D. W. Kim, P. L. Liu, H. C. Kim, J. A. Weninger, C. M. Kumar, A. Prasad, B. W. Grimsley, and H. B. Tejada, "Effects of Ag content on fracture resistance of Sn–Ag–Cu lead-free solders under high-strain rate conditions," *Mater. Sci. Eng.: A*, vols. 460–461, pp. 595–603, Jul. 2007.

[12] R. H. Dauskardt, M. Lane, Q. Ma, and N. Krishna, "Adhesion and debonding of multilayer thin film structures," *Eng. Fract. Mech.*, vol. 61, no. 1, pp. 141–162, Aug. 1998.

Jianping Jing received the Ph.D. degree from the School of Power Machinery and Engineering, Harbin Institute of Technology, Harbin, China, in 2002.

He is currently a Professor with the State Key Laboratory of Mechanical System and Vibration, School of Mechanical and Power Engineering, Shanghai Jiaotong University, Shanghai, China. He has published more than 50 research papers. His current research interests include rotor dynamics, fault diagnosis of rotary machinery, damage and reliability of mechanical structures, and vibration and noise control of mechanical systems.
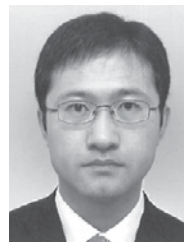
Feng Gao received the Ph.D. degree from Harbin Institute of Technology, Harbin, China.

He is currently a Research Associate in the Departments of Civil and Environmental Engineering and Mechanical Engineering, Northwestern University, Evanston, IL. His current research interests include lead-free solder alloys, reliability of interconnections, and nanostructures in microelectronic packaging.

Janine Johnson received the Ph.D. degree in mechanical engineering from Georgia Institute of Technology, Atlanta, GA, in 2009.

She is currently with the Lincoln Laboratory, Massachusetts Institute of Technology, Lexington, where she is working on solder fatigue in electronic packaging. Her current research interests include mechanics of materials, and specifically studying composites used in fuel cells.

Frank Z. Liang received the Ph.D. degree in mechanical engineering from Oregon State University, Corvallis, in 1991.

He is a Staff Engineer in the Mechanical Core Competency Group, Intel Corporation, Hillsboro, OR. He has contributed extensively to the dynamic analyses and development of mechanical shock modeling and testing methodologies for electronic components, circuit boards, and computer systems.

Dr. Frank is a fellow of the American Society of Mechanical Engineers. He has been a registered Professional Engineer since 1993.

Jianmin Qu is currently a Walter P. Murphy Professor of civil and environmental engineering and mechanical engineering at Northwestern University, Evanston, IL. His current research interests include micromechanics of composites, interfacial fracture and adhesion, fatigue and creep damage in metallic and polymer materials, thermomechanical reliability of microelectronic packaging, and ultrasonic nondestructive evaluation of advanced engineering materials. He has authored or co-authored two books and over 140 referred journal papers and book chapters in the above areas.

Richard L. Williams received the M.S. degree from Washington State University, Pullman, and the B.S. degree in applied physics from the University of Utah, Salt Lake City.

He was the Manager of the Assembly Test and Technology Development, Mechanical and Modeling Group, Intel Corporation, Hillsboro, OR, overseeing the project. He has recently transferred to Intel's Ultra Mobility Group.